Air-Sea Interaction Measurements in the West Mediterranean Sea During the Tyrrhenian Eddy Multi-Platform Observations Experiment

M. E. Schiano, R. Santoleri, F. Bignami, and R. M. Leonardi

Istituto di Fisica dell'Atmosfera, Consiglio Nazionale delle Ricerche, Rome, Italy

S. Marullo

Ente per Nuove Tecnologie l'Energia e l'Ambiente, Centro Ricerche Ambiente Marino, Rome, Italy

E. Böhm[1]

Department of Marine Earth and Atmospheric Sciences, North Carolina State University, Raleigh

Measurements of radiative fluxes were carried out in the Tyrrhenian Sea in fall and winter as part of the Tyrrhenian Eddy Multi-Platform Observations Experiment (TEMPO). These measurements have supplied the first experimental radiation data set over this basin. Seasonal variation of the different components of the budget are investigated. Since data collection was carried out in an area in which a quasi-permanent eddy is present, the behavior of the radiation parameters across the frontal zone is analyzed. The most interesting result of the air-sea interaction in proximity of a marine front consists in the covariation of sea surface temperature and downwelling long-wave radiation. Contemporaneous satellite data show a clear correlation between sea surface structure and horizontal distribution of columnar atmospheric water content. Therefore this inhomogeneity clearly is one of the main factors responsible for the variation of the downwelling radiation across the front. A comparison between experimental data and results of some of the most widely used bulk formulae is carried out for both short- and long-wave radiation. The mean difference between measured and empirical solar radiation values is less than 3%, while in the case of the net long-wave radiation budget, poor agreement is found. Indeed, a 30 W/m^2 bias results from the comparison. This discrepancy is consistent with the imbalance between previous bulk calculations of total heat budget at the surface and corresponding hydrographical observations of heat exchange at Gibraltar.

1. Introduction

The radiation budget at the sea surface, i.e., the difference between the absorbed net solar radiation and the emitted net long-wave radiation together with the fluxes of sensible and latent heat, determines the heat storage and transport in the ocean, which in turn affect the state of the atmosphere-ocean system. The space and time variability of the radiation budget is therefore central to questions of climate.

Direct high-quality radiation measurements at sea are difficult to make, and therefore only a few data have been obtained from research vessels. *Lumb* [1964], *Payne* [1972], *Reed* [1977], and *Tabata* [1964] have analyzed observations of short-wave radiation; *Charnell* [1967] reported observations of long-wave radiation near Hawaii; *Reed and Halpern* [1975] made both short-wave and net long-wave measurements off the Oregon coast; *Lind et al.* [1984], during the JASIN experiment, measured the short- and long-wave radiation terms separately in the North Atlantic; and *Lind and Katsaros* [1986] as well as *Simpson and Paulson* [1979] made the same measurements in the North Pacific.

The available information on the heat budget at the surface of the Mediterranean Sea has been mostly based upon bulk formulae applied to monthly averages of meteorological observations obtained from merchant ships. However, the accuracy of these bulk formulas for the Mediterranean Sea has never been tested. According to *Bunker et al.* [1982], the heat flux of the Mediterranean Sea calculated using the above data set is 30 W/m^2 into the sea. This figure is in poor agreement with the oceanographic observations which indicate a mean advective heat loss from the basin of 5 W/m^2 due to the currents at Gibraltar. *Bunker et al.* [1982] state that estimates of long-wave radiation fluxes are the most likely source of error in radiation balance computations. However, these authors attribute the existing imbalance between total (radiative plus turbulent) heat budget at the surface and oceanographic observations to wrong values for turbulent exchange coefficients. We feel that the question is still open, especially because there are no published measurements of radiation parameters in the Mediterranean Sea. This means that the validity of any climate study for this basin is strongly limited.

In fact, the air-sea energy exchange plays a fundamental role in the dynamics and climatology of the Mediterranean area, since the atmospheric and marine phenomenologies are strongly coupled. Strong evaporation in the basin produces a lowering of the sea level, causing a surface inflow of fresher Atlantic water and a deep outflow of saltier Mediterranean

---

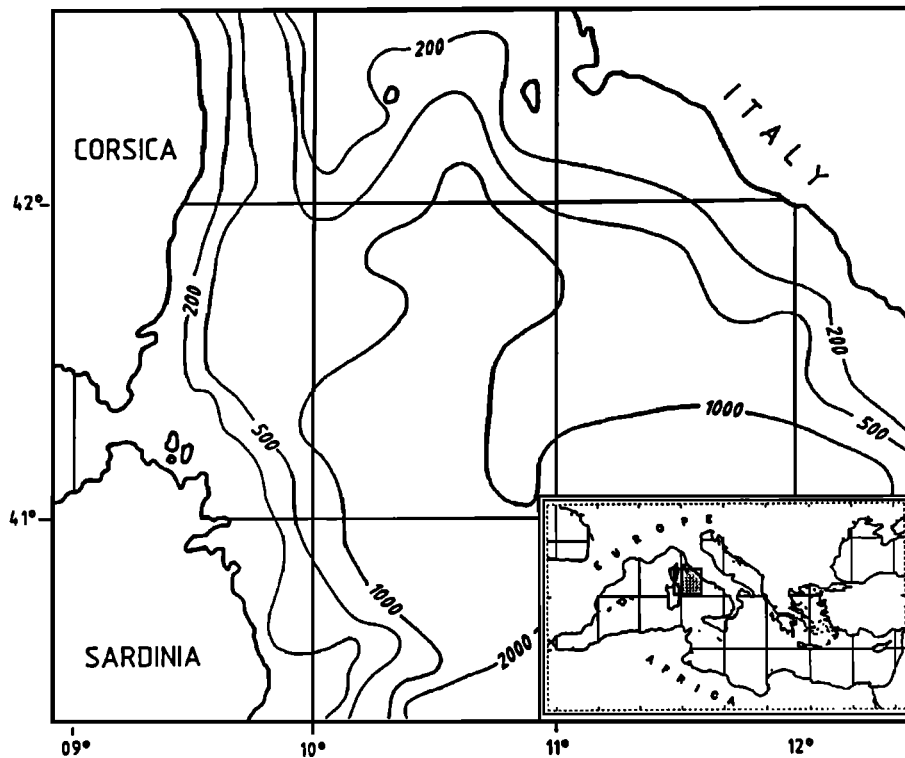[1]Permanently at Earth Observation Division, Telespazio, Rome, Italy.

Fig. 1. Bathymetry (in meters) of the north Tyrrhenian Sea showing the area of operations.

water through the strait of Gibraltar. During the winter months, winds produce intense evaporation and cooling that in some areas cause deep-water formation.

The Tyrrhenian Multi-Platform Observations (TEMPO) Experiment conducted over the north Tyrrhenian Sea provided an occasion to set up direct measurements of radiation components at sea [see TEMPO Group, 1991]. The principal aim of this project was to study the signature of a mesoscale oceanographic eddy using space-borne and airborne remote sensing and ship-based measuring techniques, but an effort was made to extend the observations to other parameters, more related to the air-sea interface phenomena. In particular, short-wave and long-wave incoming radiation and sea surface temperature were continuously measured from September 27 to October 7, 1989 (phase 1 in the following) and from February 17 to 22, 1990 (phase 2 in the following) on the R/V Minerva. The area of interest is shown in Figure 1. To overcome the difficulties in making measurements of incident radiation on board, an experimental solution was developed, based on the use of a couple of sensors for each measured term, as well as an analytical method to control the quality of the data.

In this paper, we first describe the methodologies developed to collect and process the data. Then we analyze the radiation measurements collected on board the R/V Minerva during two different periods of the year in order to study the dependence of the heat budget upon the seasons. Finally, a preliminary comparison between experimental data and empirical values obtained by the widely used bulk formulas is also reported.

2. RESEARCH CRUISES

The two cruises were made in the Tyrrhenian Sea during different periods of the year: September 27 to October 7,

1989 (phase 1) and February 17–22, 1990 (phase 2), as part of TEMPO. The region of measurements is shown in Figure 1.

Since the main objective of TEMPO was to investigate the Tyrrhenian eddy, which is a quasi-permanent elliptical eddy located to the east of Corsica and Sardinia and characterized by 150 × 100 km axes and a 2.5°C maximum temperature difference, observations during phases 1 and 2 were concentrated along the sea surface temperature (SST) front separating the eddy from the surrounding waters.

Radiation measurements were carried out continuously when the ship was either under way, at a hydrographic station, or anchored for shelter in the lee of small islands. The only rejected data were those collected in the ports.

From September 27 to 30 (first part of phase 1), a low over the Mediterranean caused moderate NE-SE winds, somewhat rough seas, highly variable cloud cover, and some rain. After September 30 the experimental area was under the influence of a high-pressure system; the sky was clear except for some diurnally evolving cloudiness, and prevailing winds blew from the north, causing variable sea state. Air temperature ranged from 17° to 25°C, while mean humidity was 70%. Cumulus and stratocumulus were the dominant cloud types observed. The typical SST difference across the Tyrrhenian eddy front was 2.0°C (Plate 1). Hydrographic measurements showed that the eddy structure extended to a depth of 200 m.

During the entire second oceanographic cruise (February 17–22, 1990) a high-pressure was present over the Mediterranean Sea. The winds, generally SE, were very weak, and the values of air temperature above average. Cloud cover was extremely variable and characterized by altostratus and cirrostratus. Hydrographic measurements show that, due to winter thermal uniformity, the SST was more uniform than

during the previous cruise (Plate 2), and the eddy structure extended to a depth of 600 m.

3. INSTRUMENTATION AND DATA ACQUISITION

The R/V *Minerva* was equipped to measure the incoming irradiance (short wave and long wave) continuously as well as the SST. Hourly observations of the principal meteorological parameters were carried out during both cruises. An Assmann psychrometer was used to make measurements of air temperature and humidity, pressure values were obtained from the ship's barometer, and the fractional cloud cover was visually estimated. All these observations were carried out from the main deck of the R/V *Minerva*, about 8 m above sea level (asl).

Short-wave irradiance was measured using two Eppley PSP pyranometers. These instruments measure the hemispheric solar irradiance in the 0.28- to 2.8-μm range. The PSP has a response time of 1 s, is compensated for temperature, and has a 2% accuracy. Long-wave irradiance was measured by two Eppley precision infrared radiometers (PIR). These pyrgeometers have mirrored silicon hemispheres with nearly constant transmittance over wavelengths ranging from 4 to 50 μm. A thermistor-resistor-battery circuit compensates for detector temperature, making the instrument accuracy better than 2%.

The PIR has a response time of the same order as the PSP.

The radiometer signals were amplified to a recording range of -5 to $+5$ V dc by amplifiers located near the sensors. Amplified signals were directed to a PC via an analog-to-digital converter (ADC) card and the data were recorded on the hard disk with a sampling time of 1 Hz and displayed on the computer screen. These four upward looking hemispheric radiometers were mounted on the upper deck of the R/V *Minerva*, about 12 m asl. The instrument locations were carefully selected to minimize the influence of the ship's structure on the measurements (i.e., avoiding having two sensors of the same kind simultaneously in the shadow of the ship's superstructure).

Every measurement system, consisting of the sensor plus its amplifier and its acquisition channel on the ADC card, was calibrated as a unit before and after each cruise. In particular, the two pyranometers were calibrated against the Italian National Standard at Vigna di Valle near Rome. In this way, the conversion factors between the raw outputs of the ADC card, expressed in digital counts, and the incident solar radiation, expressed in W/m^2, were obtained. An intercalibration test was performed to obtain the linear relationship between the two instrument systems.

In order to calibrate the two pyrgeometers, a blackbody calibration cavity was assembled in our laboratory on the basis of the Eppley calibration blackbody specifications [*Benedicti et al.*, 1990]. A test on thermal uniformity within the cavity was performed by measuring the blackbody temperature at different points. The blackbody performance was also tested against a PIR just calibrated by Eppley. The calibration was obtained by varying the blackbody temperature from 0° to 30°C and comparing the irradiance of the cavity with the output signal of each instrument system, expressed in counts. An intercalibration test was also carried out between the two PIR's and the PIR newly calibrated at Eppley.

The SST (skin) was measured by an infrared radiometer.

During the first phase of TEMPO, a PRT-5 radiometer was used, while a Minarad radiometer was employed in the second phase. Both instruments are designed to yield measurements of equivalent blackbody temperature covering the range from -20°C to $+75$°C. A spectral filter limits the measurement to the 8- to 14-μm atmospheric window. The output of both radiometers was amplified to obtain values from -5 to $+5$ V dc.

The signal was recorded on the same acquisition system used for the radiation parameters, with a sampling rate of 1 Hz. Before and after each cruise, the employed radiometer was calibrated in order to check the calibration coefficients. This radiometer was mounted on a boom over the bow of R/V *Minerva*, about 6 m asl. The SST was measured in the absence of breaking waves because in such instances the foam soaked the lens of the instrument, invalidating the readings.

4. DATA PROCESSING

The principal sources of error in these data are the background noise due to the acquisition system, shadowing of the short-wave sensors, contamination of the incoming long-wave signal by the ship's thermal field, and departure from the horizontal of all receiving surfaces due to ship pitch and roll. These errors were limited because the skyward hemisphere was occupied only by the Loran poles and both background noise and the oscillations due to the ship's pitch and roll were reduced by averaging in 1-min intervals. The use of two sensors made it possible to further reduce the errors. Since intercalibrations performed before and after the cruise indicated the absence of any systematic shift in either couple of instrument systems, any segment of data for which two instruments of the same couple did not agree must be the result of spurious data. Therefore, as the measurements from each system may generally be regarded as correct, the cases in which two systems of the same couple did not yield the same value of incident radiation must be ascribed either to a random fluctuation in one set of equipment, or to a spurious perturbation from the environment. In both cases such error sources are unlikely to affect both sets of equipment at the same instant and in the same direction.

Quality control was first carried out by excluding the data points that were outside the 95% confidence interval bands of the regression line obtained by the intercalibration of two instruments. Twenty percent of the data points were thus eliminated. The second step of the procedure was to single out the instrument responsible for the occasional failure. The following four steps were applied to the data (Figure 2).

1. For a suspect measurement interval, the temporal data segment from instrument N1 of the couple (which is suspected to yield the incorrect data) is replaced by an interpolation based on the immediately preceding and following nonsuspect segments from the same instrument.

2. The corresponding data segment of instrument N2 (which is supposed to be the correct one) is used as is.

3. Each couple made of an original value from N2 and an interpolated value from N1 is plotted with the intercalibration regression line and 95% confidence limits.

4. It is expected that if N1 is incorrect and N2 is correct, then this couple should fall within the 95% confidence limits; otherwise the opposite is likely to be true, which can be verified simply on exchanging the roles of instruments N1 and N2.
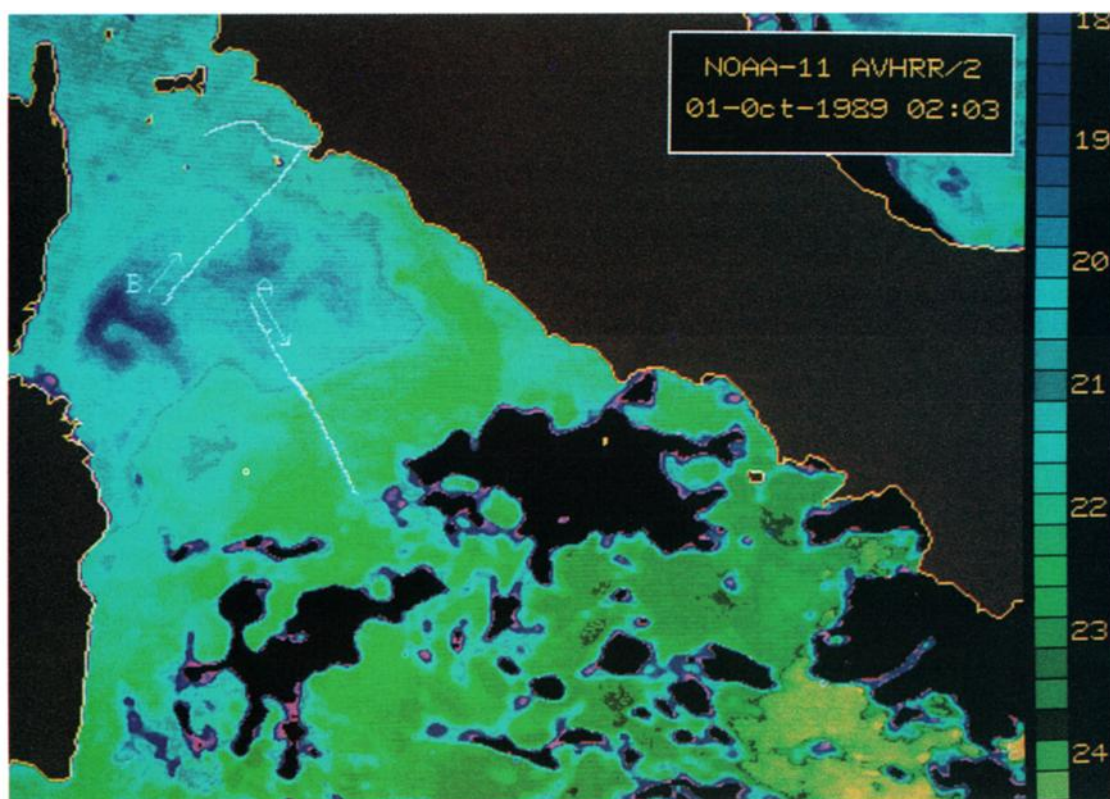
Plate 1.   AVHRR sea surface temperature map during TEMPO phase 1. Segments A and B are the routes of the ship crossing the SST front on October 1 and 3, 1989, respectively.
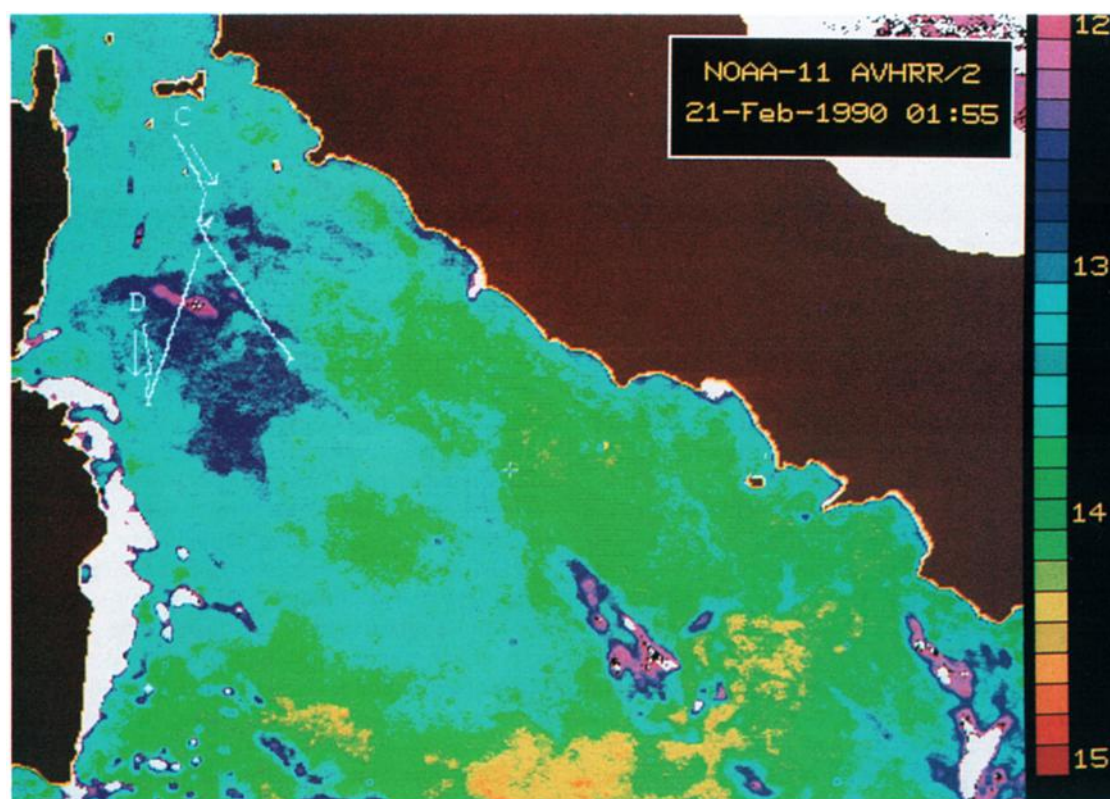

Plate 2.   AVHRR sea surface temperature map during TEMPO phase 2. Segments C and D are the routes of the ship crossing the SST front on February 17 and 21, 1990, respectively.
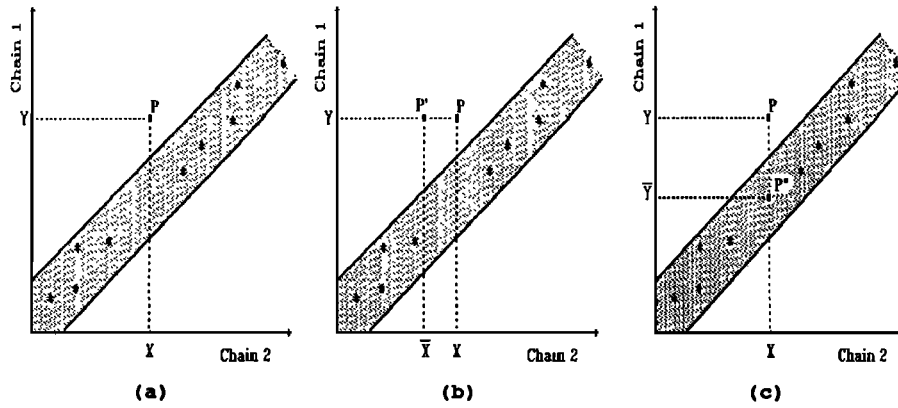
Fig. 2. Sketch of quality control technique used for data recorded with two sensors. (*a*) The 95% confidence region of the intercalibration regression. Point P(X, Y) lies out of the confidence band and therefore is a suspect couple of values. (*b*) P'($\bar{X}$, Y) is the couple obtained by replacing X by an interpolation $\bar{X}$ using the data recorded immediately before and after X. Since P' still lies out of the band, (*c*) the same check is performed on the other instrument system with point P"(X, $\bar{Y}$). If P" lies in the band, X is correct and Y is rejected. If not, both will be rejected.

By applying this procedure, 60% of the data rejected from the first discrimination criterion was recovered. Averaging the output signals over 1 min, the background noise was eliminated.

The analysis of the distribution in time of the rejected data indicated that while the data loss was negligible for long-wave radiation, the short-wave record contained several time intervals of a few minutes for which there were no data. In order to construct a radiation data set as complete as possible, interpolation of the solar radiation was adopted to fill gaps using the method suggested by *Lind and Katsaros* [1986].

This method assumes that a better estimate can be obtained by linearly interpolating transmittance instead of short-wave irradiance ($E_s \downarrow$), since the variability of the former parameter is smoother than that of the latter. To interpolate $E_s \downarrow$, short-wave transmittance τ is calculated during 30-min periods before and after the interval without data. Transmittances are linearly interpolated for gap periods, and estimates of $E_s \downarrow$ are calculated using solar zenith angles θ, the solar constant E_{so}, and interpolated transmittances τ^* as

$$E_s \downarrow = E_{so}\tau^* \cos \theta$$

Gautier and Katsaros [1984] show that combined measured and interpolated errors in $E_s \downarrow$ are of the order of 10% in absolute irradiance values.

The SST is computed from the radiometer measurements converting the output counts to degrees Celsius. Long-wave upward radiation $E_l \uparrow$ was then computed from the SST using the Stefan-Boltzmann law:

$$E_l \uparrow = \varepsilon\sigma T^4 + \rho E_l \downarrow$$

where $E_l \downarrow$ is atmospheric radiation, ε is water emittance (0.98), ρ is long-wave reflectance (0.045), σ is the Stefan-Boltzmann constant, and T is SST. Values for ε and ρ were taken from *Mikhaylov and Zolotarev* [1970].

5. DATA

Figures 3 and 4 show 1-min averaged radiation components and the radiation budget during phases 1 and 2 of

TEMPO, respectively. Tables 1 and 2 list daily mean radiation components and radiation budget for the first and the second cruise, respectively. The meteorological data are provided in Tables 3 and 4.

The solar radiation defines the diurnal behavior of the net radiation budget and offsets the sea heat loss due to the infrared radiation budget. During the first cruise, the mean daily values of incident solar radiation ranged from 86 to 214 W/m². Nevertheless, it must be noted that the data on September 28 and 29 were altered by rain. Due to a strong northerly wind, starting from October 1 the sky became clear, although a thin layer of clouds was sometimes present around midday. The daily mean value of solar radiation for the last period of this cruise was about 200 W/m², and a maximum of 214 W/m² was recorded on October 1.

During the second cruise, only for one day, February 21, the sky was very clear, and the incident solar radiation was about 163 W/m². All the other days were characterized by high cloudiness, especially around midday, but it never rained. Therefore, in addition to the seasonal reduction, the low daily mean values of the second cruise result also from cloudiness.

The reflected short-wave radiation gives a very small contribution to the radiative budget. The maximum mean daily value obtained from both cruises was about 15 W/m², i.e., about 1 order of magnitude smaller than all the other terms. No differences were observed between reflected short-wave data obtained during the two phases.

The day-to-day variation of atmospheric radiation is greater (about 40 W/m²) than the difference between the mean values of the two cruises: the mean daily value ranged from 302 to 360 W/m² during phase 1 and from 296 to 345 W/m² during phase 2. For both cruises the lower values were recorded in very clear sky conditions. Cloudiness produced the greatest effects on the downwelling infrared radiation variability.

The variability of the infrared upwelling radiation is clearly influenced by the horizontal SST heterogeneity of the investigated area. Therefore the mean daily values of infrared radiation emitted by the sea were about 430 W/m² during phase 1, but jumps of about 30 W/m² were recorded passing through the marine front. The seasonal decrease in SST
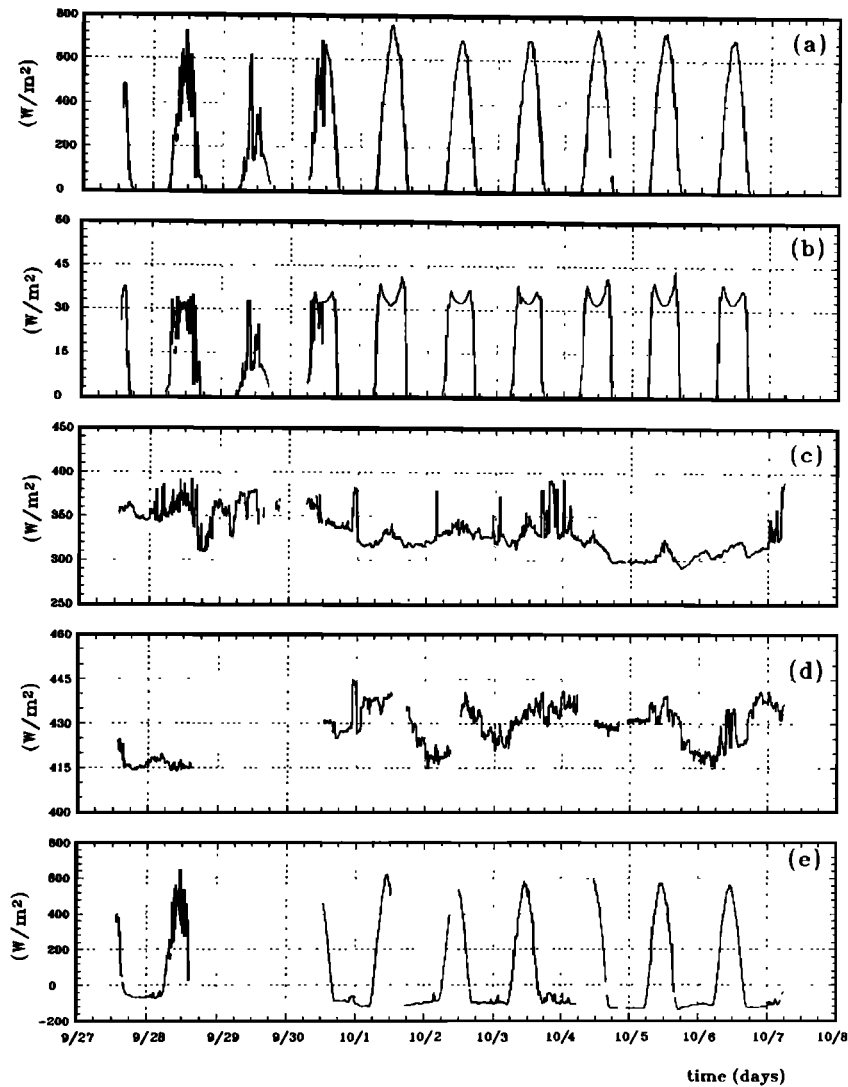
Fig. 3. Time series of 10-min averages of the various radiative components during TEMPO phase 1: (a) incident solar radiation, (b) upward solar radiation, (c) downwelling long-wave radiation, (d) upwelling long-wave radiation, and (e) net radiation budget. Time is expressed in month/day.

determines the difference between the values of the two cruises. The wintertime attenuation of the thermal gradient across the marine front causes a more uniform horizontal distribution of the upwelling radiation data. Indeed, the mean daily value obtained during the second cruise was about 390 W/m² and the variation was about 10 W/m² only, except when the Ligurian front was crossed.

Finally, the net radiation budget was computed. It ranged from about 87 to 62 W/m² during phase 1, while it was quite constant, about 55 W/m², during phase 2. A clear seasonal trend emerges from the comparison between the data of the two cruises. Indeed, the seasonal reduction of solar radiation is only partly counterbalanced by the decrease in upwelling infrared radiation. A slight decrease of the net radiation budget occurred during phase 1, caused by the decrease of atmospheric radiation associated with reduced cloudiness.

A closer look at the long-wave terms reveals that atmospheric radiation variations were often concurrent with changes in upwelling infrared radiation. This concurrence was particularly evident during the second cruise, even if there was no clear correspondence between the magnitude of the two

variations. Since, when passing through fronts, the upwelling and downwelling infrared radiation undergo variations of different magnitude, the crossing effect was also evident in the net radiation budget, especially in the nocturnal values recorded during the second cruise. The geographical location of these events indicates that the ship was crossing the edge of the Tyrrhenian eddy. To show this, we have superimposed the route of the ship on the available advanced very high resolution radiometer (AVHRR) images every time in which this phenomenon occurs. In Figure 5 we show two examples of observed simultaneous jumps in SST and downwelling radiation for each cruise. The corresponding segments of the ship's route are drawn over the AVHRR images in Plates 1 and 2.

Note that even if marine thermal gradients were reduced in amplitude during the second cruise, the corresponding variations in downwelling radiation are larger than those encountered during the first cruise. This could be due to the enhanced temperature difference between air and water observed during phase 2 (3°C in February versus 1°C in October).

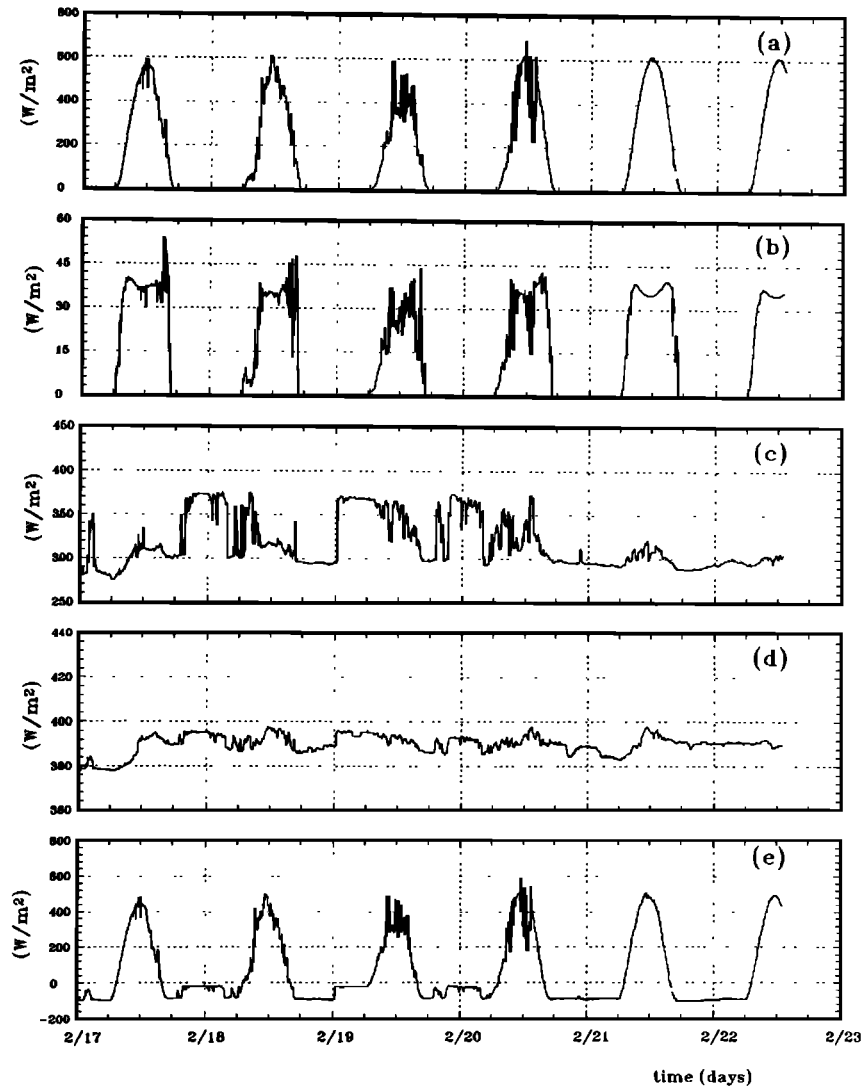The downwelling infrared radiation depends on the entire inhomogeneous atmospheric column. Its variability must be

Fig. 4. Time series of 10-min averages of the various radiative components during TEMPO phase 2: (a) incident solar radiation, (b) upward solar radiation, (c) downwelling long-wave radiation, (d) upwelling long-wave radiation, and (e) net radiation budget. Time is expressed in month/day.

attributed to a change in the air mass. The variation in SST corresponds to a change in the water mass features. Therefore, every time that contemporaneous changes in atmospheric radiation and SST were observed, the ship was crossing not only a marine front but also a discontinuity in the atmospheric characteristics.

The availability of AVHRR satellite images relative to the periods of the cruises led us to check this inhomogeneity of the air masses on either side of marine fronts in the following way. Since the difference between channels 4 and 5 of the AVHRR is proportional to the columnar water vapor content [Dalu et al., 1985; Dalu, 1986], we were able to obtain maps of this latter quantity using the algorithm developed by Dalu [1986]:

TABLE 1. Mean Daily Values of Radiation Budget Components During TEMPO Phase 1

Time	$E_s \downarrow$	$E_s \uparrow$	$E_l \downarrow$	$E_l \uparrow$	E_{net}
Sept. 28	152.2	10.1	351.4	415.9	77.6
Sept. 29	86.9	5.3	360.0	—	—
Sept. 30	180.2	12.7	347.7	429.9	85.3
Oct. 1	214.3	14.8	320.5	433.0	87.0
Oct. 2	192.2	13.4	330.3	425.7	83.4
Oct. 3	190.6	13.5	336.6	431.1	82.6
Oct. 4	206.7	13.9	317.5	431.5	78.8
Oct. 5	204.0	14.7	301.9	429.5	61.7
Oct. 6	193.7	14.5	311.3	426.9	63.6

Units are W/m².

TABLE 2. Mean Daily Values of Radiation Budget Components During TEMPO Phase 2

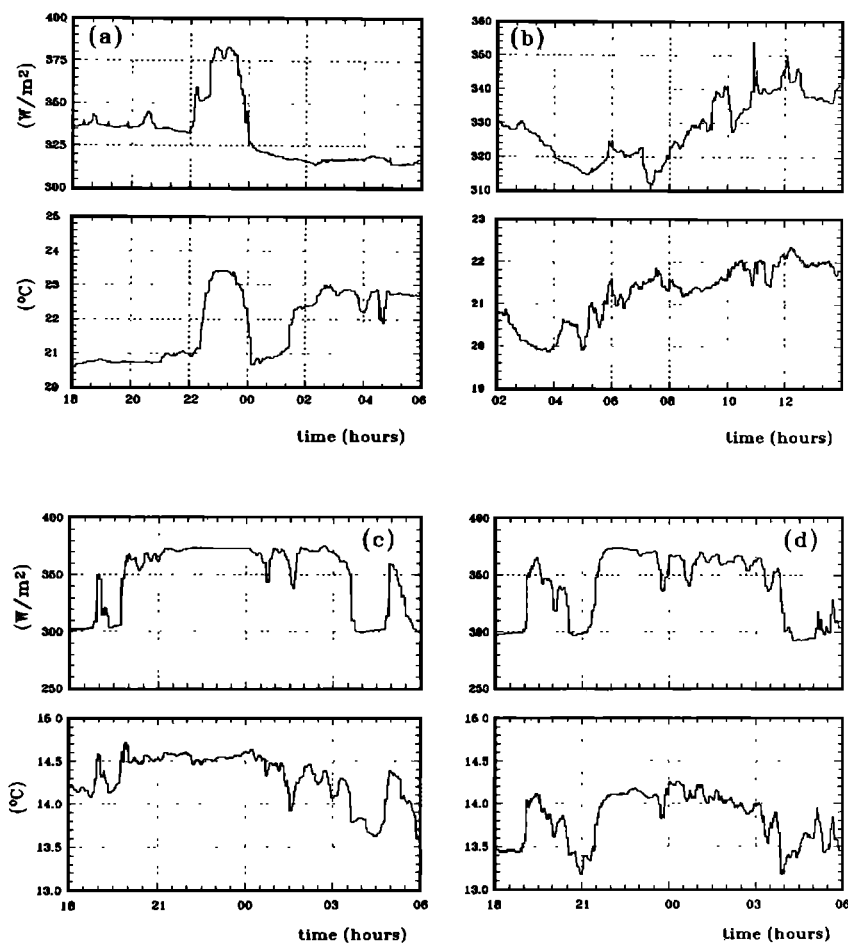| Time	$E_s \downarrow$	$E_s \uparrow$	$E_l \downarrow$	$E_l \uparrow$	E_{net}
Feb. 17	145.4	14.7	311.1	386.4	55.4
Feb. 18	134.6	11.6	319.2	390.5	51.7
Feb. 19	114.2	9.0	345.4	391.5	59.1
Feb. 20	140.7	11.7	320.3	390.0	59.3
Feb. 21	163.7	14.1	296.3	389.2	56.7
Feb. 22	—	—	297.4	390.1	—

Units are W/m².

Fig. 5. Time series of SST (lower panel) and downwelling long-wave radiation (upper panel) across the Tyrrhenian eddy front: (a and b) TEMPO phase 1 data relative to tracks A and B (October 1 and 3, 1989) in Plate 1 and (c and d) TEMPO phase 2 data relative to tracks C and D (February 17 and 21, 1990) in Plate 2.

$$W = 1.96(T_4 - T_5)$$

where T_4 and T_5 are brightness temperatures measured by channels 4 and 5 of the AVHRR. This was done for all the images which were free of clouds, relative to the area and period of the observed simultaneous jumps in SST and downwelling infrared radiation. As an example, the obtained images relative to the data of Figures 5b and 5c are shown in Plates 3 and 4, in which we also display the SST map relative to the same satellite pass obtained by using the McClain et al. [1985] algorithm.

The resulting images show a clear correlation between

SST and water vapor structures. In particular, in the zone of the cold eddy the columnar water vapor content is inferior to that of the warmer surroundings (Plates 3 and 4). Typically, values of water vapor content ranged between 2.4 g/cm^2 within the eddy and 3.2 g/cm^2 outside for the first cruise, while 1.5–2.3 g/cm^2 was the corresponding range measured in phase 2.

Since the Tyrrhenian eddy is a quasi-permanent structure of this basin, it is clear that this correlation is due to the influence of this marine feature on the overlying air mass, provided that the residence time of the latter over the eddy is sufficiently long. Nicholls et al. [1982], using a three-dimensional model, found that the mean properties of the marine atmospheric boundary layer will adjust on a time

TABLE 3. Mean Daily Values of Meteorological Data During TEMPO Phase 1

Time	T_{air}, °C	T_{sea}, °C	U, %	C, oktas
Sept. 28	21.0	18.1	72	4
Sept. 29	19.0	—	71	6
Sept. 30	20.3	20.7	76	4
Oct. 1	20.5	21.4	63	1
Oct. 2	20.7	20.1	68	1
Oct. 3	20.4	21.0	74	1
Oct. 4	—	21.2	—	0
Oct. 5	19.1	21.0	54	0
Oct. 6	19.9	20.4	59	0

TABLE 4. Mean Daily Values of Meteorological Data During TEMPO Phase 2

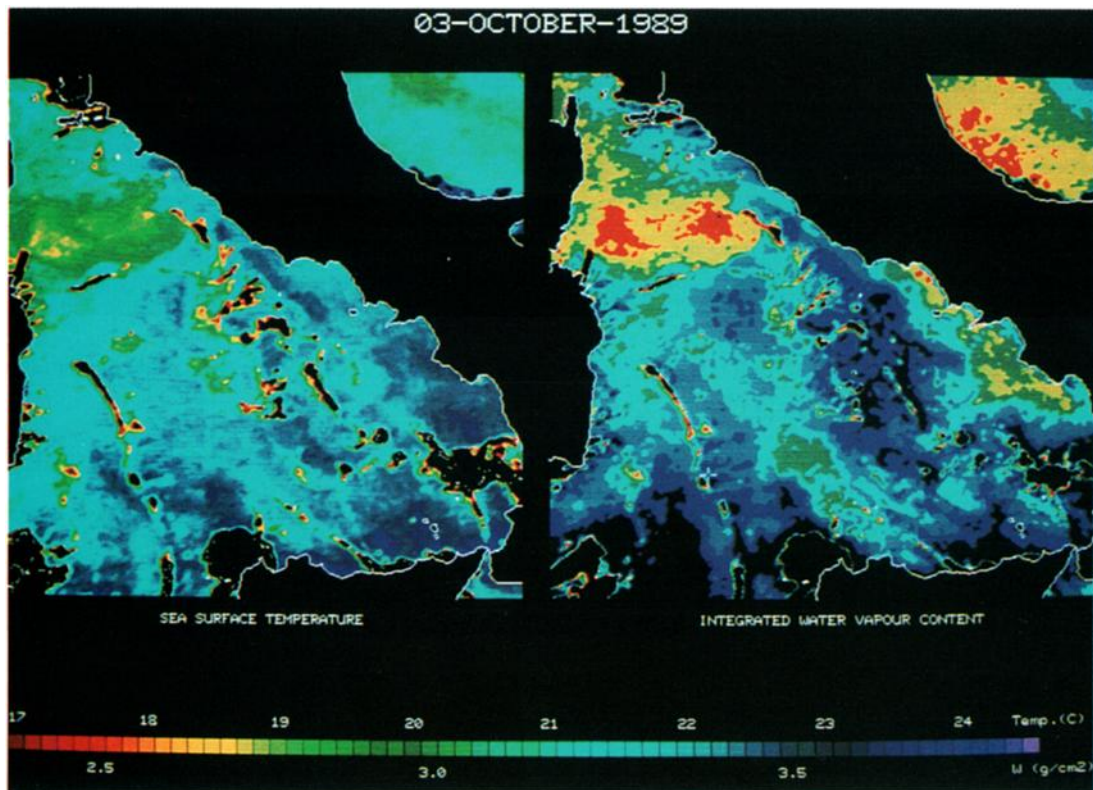| Time	T_{air}, °C	T_{sea}, °C	U, %	C, oktas
Feb. 17	16.6	13.0	82	3
Feb. 18	16.3	13.7	86	4
Feb. 19	16.1	13.6	85	7
Feb. 20	15.9	13.6	87	4
Feb. 21	15.2	13.6	88	1
Feb. 22	15.3	13.8	88	0

Plate 3. Maps of SST (left panel) and integrated water vapor content (right panel) during TEMPO phase 1. Images are relative to October 3, 1989 (track B in Plate 1 and Figure 5b.)
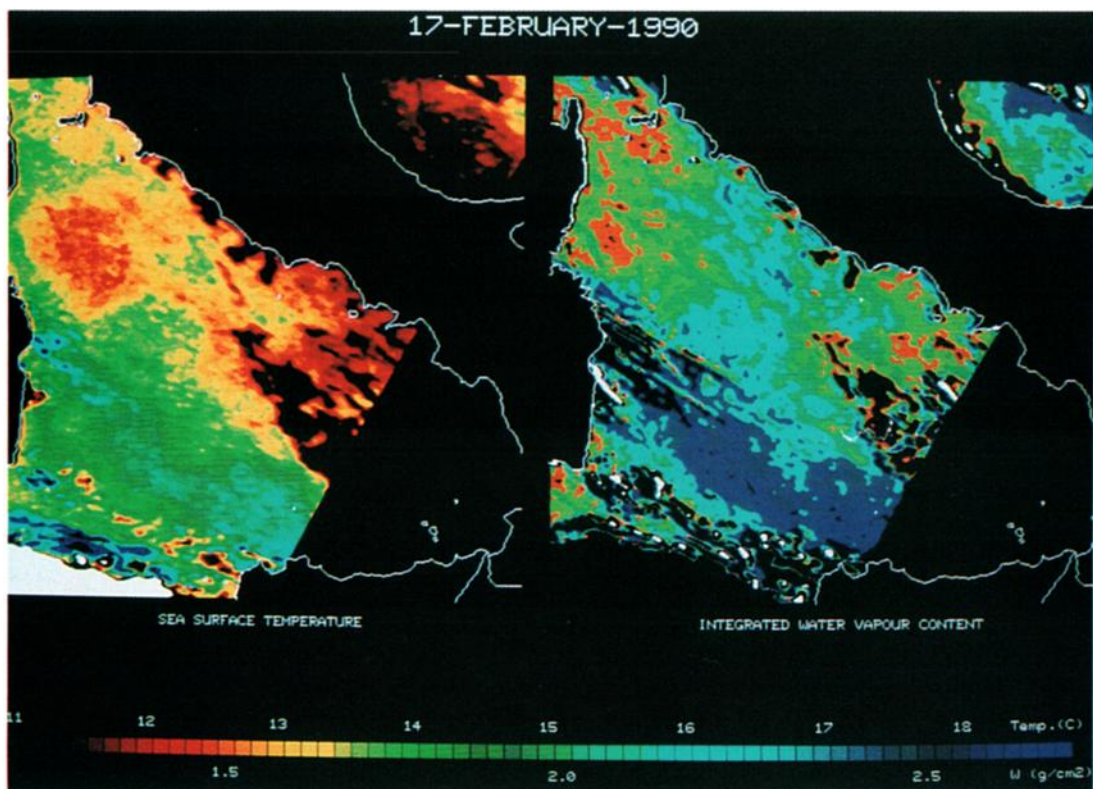

Plate 4. Maps of SST (left panel) and integrated water vapor content (right panel) during TEMPO phase 2. Images are relative to February 17, 1990 (track C in Plate 2 and Figure 5c).

TABLE 5. Comparison Between Measured Mean Daily Shortwave Incoming Radiation Data and Bulk Formula Estimates During TEMPO Phase 1 Together With Diurnal Mean Cloud Cover Values

Time	Measured	Lumb	Reed	C, oktas
Sept. 27	46.6	41.7	—	3
Sept. 28	152.2	149.9	151.5	5
Sept. 29	86.9	72.7	114.7	7
Sept. 30	180.2	108.8	178.9	3
Oct. 1	214.3	230.5	211.5	0
Oct. 2	192.2	222.0	206.2	0
Oct. 3	190.6	206.3	202.2	0
Oct. 4	206.7	203.8	204.3	0
Oct. 5	204.0	215.8	201.3	0
Oct. 6	193.7	211.3	196.9	0

Units are W/m^2 unless otherwise noted.

scale of a day after an initial perturbation at the air-sea interface, i.e., a change in the SST beneath the air column. Evidence of modifications in the humidity profiles is found within 3 hours from the occurrence of the perturbation. This implies that if air masses are slow enough to reside over the eddy for more than a few hours, the water vapor profiles should be significantly modified.

6. PARAMETERIZATION

Several formulae have been proposed to compute the radiative fluxes: some require as input only the surface weather observations, and some also use the upper air data at standard synoptic levels. Since the principal aim of empirical formulas should be the estimation of a hard-to-measure parameter using routine observations, in the present work, we have only analyzed the simpler formulations developed and/or tested at sea.

The bulk formulas chosen to predict the solar radiation are due to *Lumb* [1964] and *Reed* [1977]. Lumb's formula gives the hourly value of the solar radiation $E_s \downarrow$ starting from a division of the sky cover into nine categories. For each category, the following is used:

$$E_s \downarrow = (a + bS)SE_{so}$$

where E_{so} is the solar constant, a and b are constants for each cloud category, and S is the mean cosine of the solar zenith angle at the beginning and end of the hour for which the insolation is calculated. Predictions of Lumb's formula were made for each hour of the day and then averaged to obtain a daily value.

Reed's relation estimates the daily mean insolation using the Smithsonian tables [i.e., *Seckel and Beaudry*, 1973] for clear sky radiation and the following formula for the attenuation by clouds:

$$E_s \downarrow = (1 - 0.62C + 0.0019\alpha)E_{cs}$$

where E_{cs} is the clear sky radiation, C the daily mean fractional cloud cover, and α the solar elevation at noon. Reed's formula was used with the average daytime cloud cover. The noon solar elevation was calculated from the daily latitude value.

Comparison between the results of these two empirical formulas and the experimental data is shown in Tables 5 and 6 for TEMPO phases 1 and 2, respectively. For clear sky,

Reed's prediction is closer to the experimental data than Lumb's. Under cloudy conditions the opposite occurs, even though both formulae underestimate solar radiation. This underestimate on overcast days might be due to errors in the visual estimation of fractional cloud cover. The accuracy of cloud cover estimates is difficult to quantify because it depends on the single observer. Especially during phase 2, when the cloud cover was variable, the observation of this parameter became very critical. Measured intensities higher than predicted with partially overcast sky may also result from the clouds reflecting extra radiation downward when the sun was not obscured. In the vicinity of the coasts, cumulus clouds might have increased insolation for low zenith angles. From the practicality standpoint, Lumb's formula is less practical than Reed's for use with shipboard routine observations, since both cloud amount and cloud type are required.

All the bulk formulas used to predict the net long-wave radiation require as input the same parameters, namely, routine surface observations, and therefore can be employed in climatological work. Here we tried some of the formulas most widely used by oceanographers (Table 7).

Experimental values of net long-wave radiation at the sea surface were compared with the empirical results obtained using these bulk formulas (Figure 6). In order to make a comparison between direct measurements and bulk formula estimates of net long-wave radiation, only the data collected concurrently with the weather observations could be exploited. Therefore the downwelling and upwelling radiation data were averaged over a 10-min interval centered on the weather observation times. A comparison of the experimental data points with the results obtained using the examined bulk formulas is shown in Figure 6 as a time series. By visually inspecting the latter, it is clear that the bulk formulas underestimate the measured values of infrared budget by approximately 30 W/m^2 (Tables 8 and 9). This bias is independent of cloud cover and therefore indicates that the bulk formulas underestimate is not due to errors in cloud cover observations.

7. DISCUSSION AND CONCLUSIONS

From the point of view of heat exchanges between air and sea, the Mediterranean Sea is still scarcely understood. The evaluation of the influence of the sea upon the atmosphere is greatly complicated by the presence of high mountains surrounding the sea and of mountainous islands within the sea. Therefore the estimation of the importance of air-sea

TABLE 6. Comparison Between Measured Mean Daily Shortwave Incoming Radiation Data and Bulk Formula Estimates During TEMPO Phase 2 Together With Diurnal Mean Cloud Cover Values

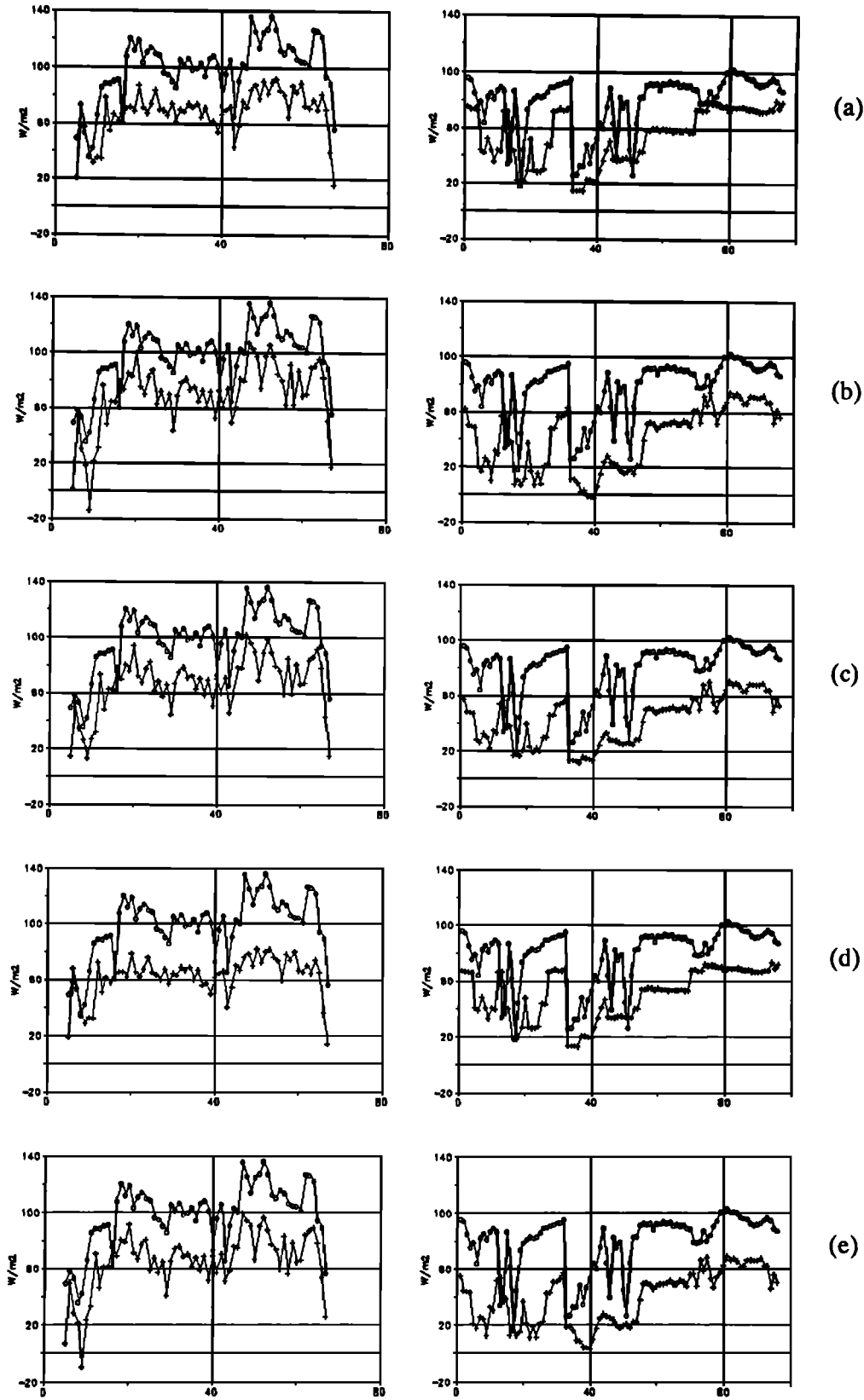| Time	Measured	Lumb	Reed	C, oktas
Feb. 17	145.4	124.5	111.9	4
Feb. 18	134.6	99.3	97.6	6
Feb. 19	114.2	100.6	85.4	7
Feb. 20	140.7	127.7	112.8	5
Feb. 21	173.7	170.7	167.4	0
Feb. 22	138.6	124.0	—	0

Units are W/m^2 unless otherwise noted.

Fig. 6. Comparison between measured net long-wave radiation budget (circles) and bulk formula estimates (crosses). Left panels are relative to TEMPO phase 1, and the right panels are relative to TEMPO phase 2. The data are in chronological order, although data gaps have been omitted: (a) Brunt [1932], (b) Berliand and Berliand [1952], (c) Anderson [1952], (d) Efimova [1961], and (e) Bunker [1976].

TABLE 7.   List of Bulk Formulas Used for Net Long-Wave Budget Estimates

Net Long-Wave Radiation	$E_{net_l} = E_l \uparrow - E_l \downarrow$
Brunt [1932]	$E_{net_l} = \varepsilon\sigma T_s^4[0.39 - 0.05\sqrt{e_a}]F(C)$
Berliand and Berliand [1952]	$E_{net_l} = \varepsilon\sigma T_a^4[0.39 - 0.05\sqrt{e_a}]F(C) + 4\varepsilon\sigma T_a^3(T_s - T_a)$
Anderson [1952]	$E_{net_l} = \varepsilon\sigma[T_s^4 - T_a^4(0.74 + 0.0049e_a)]F(C)$
Efimova [1961]	$E_{net_l} = \varepsilon\sigma T_a^4[0.254 - 0.00495e_a]F(C)$
Bunker [1976]	$E_{net_l} = \varepsilon\sigma T_a^4[0.257 - 0.0051e_a](1 - 0.68C) + 4\varepsilon\sigma T_a^3(T_s - T_a)$

T_s, sea surface temperature; σ, Stefan-Bolzmann constant; ε, sea surface emissivity (0.98), T_a, air temperature (in degrees Kelvin); e_a, near-surface vapor pressure (in millibars); C, fractional cloud cover (in tenths); and $F(C) = 1 - 0.8C$, cloud correction factor.

heat exchange with respect to the climate of the entire basin is critical.

Measurements of incident short-wave and downwelling long-wave radiation and of SST were carried out during two cruises in the north Tyrrhenian Sea in fall and winter. These measurements have supplied the first experimental radiation data set over this basin. A quality control technique based on a redundant number of sensors proved very effective in reducing data loss. As a result, a continuous time series of incoming radiation measurements was obtained for both cruises.

Evidence of seasonal variation was expected and found in both incident solar radiation and upwelling long-wave radiation. An unusually high air temperature during the second cruise (February 1990) partially reduced the expected seasonal dependence of the downwelling long-wave radiation. Nevertheless, the radiation budget (i.e., upwelling minus downwelling long-wave radiation) in February 1990 decreased by about 25 W/m² with respect to the October 1989 budget.

Since data collection was carried out with the ship steaming, it was possible to observe the behavior of the radiation parameters while traversing SST fronts. The most interesting example of air-sea interaction in the proximity of a marine front consisted of the covariation of SST and downwelling long-wave radiation. We think that this phenomenon results from the influence of the sea on the overlying atmosphere: different temperatures on either side of a permanent front such as the Tyrrhenian eddy give rise to different evaporative fluxes. These in turn cause horizontal inhomogeneity in the atmospheric distribution of water vapor. Since water vapor is the greatest contributor to the downwelling infrared radiation, these horizontal gradients in downwelling infrared radiation colocated with sufficiently intense SST fronts are expected to occur in the ocean. In order to test the above hypothesis on the horizontal distribution of water vapor induced by marine thermal fronts, we computed maps of vertically integrated water vapor from AVHRR data. We used an algorithm based on the assumption that this quantity is proportional to the difference

between brightness temperatures measured in the two adjacent spectral IR channels of the AVHRR [Dalu, 1986]. From radiative transfer calculations, Dalu [1986] estimates the error in computing vertically integrated water vapor content to be 0.15 g/cm².

The resulting maps (Plates 3 and 4) show a close resemblance between marine thermal structures and atmospheric water vapor distribution. We can reject the observed front as being due to the atmospheric correction algorithm used to obtain absolute values of SST because the presence of the marine thermal front was independently measured by the onboard infrared radiometer.

On the other hand, since $T_4 - T_5$ also depends on the SST, one might argue that the differences in water vapor content we estimated across the marine front are fictitious and due only to the front itself. We have therefore estimated the shift in $T_4 - T_5$ in an ideal case where an SST front was present in the absence of horizontal water vapor content gradients. In fact, we assumed a "worst case" with a 3°C jump across the front, which is well above the maximum observed values, and a uniform water vapor content set to 3.5 g/cm², which also is an extremal value for the Italian seas [Dalu et al., 1985]. In this case the differences in $T_4 - T_5$ values across the front lead to a maximum fictitious jump in water vapor content of about 0.3 g/cm². Therefore the estimated 0.8 g/cm² (Plates 3 and 4) cannot be fictitious and is due to a real inhomogeneity in the horizontal distribution of the atmospheric columnar water vapor content.

A comparison between experimental data and results of some of the most widely used bulk formulas was also carried out for both short and long waves. In the case of incident solar radiation, the mean difference between measured data and bulk formula estimates is less than 3%, even though there is considerable scatter (an average rms error of about 22 W/m², i.e., about 14%), especially in the cases of partial cloud cover and broken clouds. We think that, in this case, bulk formulas underestimate the insolation because the extra downward radiation reflected by the cloud edges is not accounted for.

TABLE 8.   Comparison Between Bulk Net Long-Wave Budget Estimates and Direct Measurements During TEMPO Phase 1

	Mean Bias Error, W/m²	rms Error, W/m²
Brunt [1932]	29.2	32.2
Berliand and Berliand [1952]	28.5	31.5
Anderson [1952]	31.2	33.6
Efimova [1961]	35.7	38.7
Bunker [1976]	32.6	34.9

TABLE 9.   Comparison Between Bulk Net Long-Wave Budget Estimates and Direct Measurements During TEMPO Phase 2

	Mean Bias Error, W/m²	rms Error, W/m²
Brunt [1932]	25.8	29.8
Berliand and Berliand [1952]	38.1	42.1
Anderson [1952]	36.1	39.1
Efimova [1961]	28.6	32.1
Bunker [1976]	39.3	42.7

In the case of the net long-wave radiation budget, we found poor agreement between experimental data and empirical values: the data computed from all bulk formulas show a bias of about -30 W/m^2 with respect to the measured budget (Table 2). The rms error is above 30 W/m^2, giving an uncertainty in the computed values of about 40%. This rms error is therefore mainly due to the cited bias. In fact, the empirical estimates seem to follow the short-period oscillations of the experimental data reasonably well.

The observed bias cannot be due to a systematic error in the measurements of the long-wave downwelling radiation caused by the ship's thermal field. In fact, if that were the case, the difference between the infrared upwelling and downwelling radiation should be made more negative as a result of the increase in the measured downwelling component due to the ship's thermal emission. Therefore, if the bulk formulas were correct, their estimate should be higher than the observations, which is exactly the opposite of what we found.

Another source of systematic error could come from solar heating of the radiometer dome that can, when not properly compensated, produce an overestimation of the downwelling long-wave radiation as high as 90 W/m^2 [Alados-Arboledas et al., 1988; Enz et al., 1975; Weiss, 1981; Ryznar and Weber, 1982; Bréon et al., 1991]. In this case the error acts in the same direction as the ship's effect. Moreover, since this bias is always observed independently of the time of the day, it cannot be attributed to a diurnal effect.

Finally, we can definitely reject the fact that such a systematic error could be instrument induced, because no bias was observed between the two pyrgeometers located 1 m apart and individually calibrated before and after each cruise [Bréon et al., 1991]. We can also exclude offsets induced in the calibration phase, since the blackbody cavity was successfully tested on more than one occasion (see section 3). It appears as though this discrepancy is due to the weight that each parameter has in the bulk formulas. Adjusting the coefficients should make it possible to improve the estimate of the long-wave radiation budget at the sea surface, but this requires a data set larger than the present one. We feel that this adjustment is necessary, since the bulk formulas were developed using observations over land; therefore the application of these formulas at sea can cause systematic errors due to the different atmospheric conditions.

In fact, the long-wave radiation budget is strongly affected by the profile of water vapor and the liquid water path over the whole atmospheric column. The values of the water vapor content in the lower atmosphere significantly vary from land to sea. Therefore the use of surface water vapor pressure values obtained over the sea together with coefficients determined over land can produce an overestimation of the columnar water vapor with a consequent overestimation of the downwelling infrared radiation. This obviously leads to an underestimation of the budget, intended as upwelling minus downwelling long-wave radiation, which is what we observe for most cases. A new determination of the coefficients for marine measurements is therefore necessary.

In conclusion, the absence of bias in the incident solar radiation parameterization with respect to observations, combined with the evidence of a large bias in the net long-wave budget with respect to observations, suggests that corrections are to be sought mainly for long-wave rather than short-wave bulk formulas. Moreover, we note that the 35 W/m^2 discrepancy found for the Mediterranean Sea by Bunker [1972] and Bunker et al. [1982] between the surface heat flux over the entire basin and the heat flux due to the water mass exchange at Gibraltar has both sign and magnitude consistent with our results.

REFERENCES

Alados-Arboledas, L., J. Vida, and J. I. Jiménez, Effect of solar radiation on the performance of pyrgeometers with silicon domes, J. Atmos. Oceanic Technol., 5, 666–670, 1988.

Anderson, E. R., Energy budget studies, U.S. Geol. Surv. Circ., 229, 71–119, 1952.

Benedicti, G., R. M. Leonardi, R. Santoleri, and M. E. Schiano, Realizzazione di un sistema per la calibrazione dei pirgeometri, Ref. 90-39, 8 pp., Ist. di Fis. dell'Atmos., Cons. Naz. delle Ric., Rome, Italy, 1990.

Berliand, M. E., and T. G. Berliand, Measurement of the effective radiation of the Earth with varying cloud amounts (in Russian), Izv. Akad. Nauk. SSSR, Ser. Geofiz., 1, 1952.

Bréon, F. M., F. Frouin, and C. Gautier, Downwelling longwave irradiance at ocean surface: An assessment of in situ measurements and parameterization, J. Appl. Meteorol., 30, 17–31, 1991.

Brunt, D., Notes on radiation in the atmosphere, Q. J. R. Meteorol. Soc., 58, 389–420, 1932.

Bunker, A. F., Wintertime interactions of the atmosphere with the Mediterranean Sea, J. Phys. Oceanogr., 2, 225–238, 1972.

Bunker, A. F., Computation of surface energy flux and annual air-sea cycle of the North Atlantic Ocean, Mon. Weather Rev., 104, 1122–1140, 1976.

Bunker, A. F., H. Charnock, and R. A. Goldsmith, A note on the heat balance of the Mediterranean and Red seas, J. Mar. Res., 40, Suppl., 73–84, 1982.

Charnell, R. L., Long-wave radiation near Hawaiian Island, J. Geophys. Res., 72, 489–495, 1967.

Dalu, G., Satellite remote sensing of atmospheric water vapour, Int. J. Remote Sens., 7(9), 1089–1097, 1986.

Dalu, G., A. Viola, and S. Marullo, Sea surface temperature from AVHRR-2 data, Nuovo Cimento, 8C(6), 793–804, 1985.

Efimova, N. A., On methods of calculating monthly values of net longwave radiation (in Russian), Meteorol. Gidrol., 10, 28–33, 1961.

Enz, J. W., J. C. Klink, and D. G. Baker, Solar radiation effect on pyrgeometer performance, J. Appl. Meteorol., 14, 1297–1302, 1975.

Gautier, C., and K. B. Katsaros, Insolation during STREX, 1, Comparison between surface measurements and satellite estimates, J. Geophys. Res., 89, 11,778–11,788, 1984.

Lind, R. J., and K. B. Katsaros, Radiation measurements and model results from R/V Oceanographer during STREX 1980, J. Geophys. Res., 91(D12), 13,308–13,314, 1986.

Lind, R. J., K. B. Katsaros, and M. Gube, Radiation budget components and their parameterization in JASIN, Q. J. R. Meteorol. Soc., 110, 1061–1071, 1984.

Lumb, F. E., The influence of clouds on hourly amounts of total solar radiation at the sea surface, Q. J. R. Meteorol. Soc., 90, 43–56, 1964.

McClain, E. P., W. G. Pichel, and C. C. Walton, Comparative performance of AVHRR-based multichannel sea surface temperatures, J. Geophys. Res., 90(11), 11,587–11,601, 1985.

Mikhaylov, B. A., and V. M. Zolotarev, Emissivity of liquid water, Izv. Akad. Sci. USSR Atmos. Oceanic Phys., Engl. Transl., 6, 52, 1970.

Nicholls, S., M. A. LeMone, and G. Sommeria, The simulation of a fair weather marine boundary layer in GATE using a three-dimensional model, *Q. J. R. Meteorol. Soc.*, *108*, 167–190, 1982.

Payne, R. E., Albedo of the sea surface, *J. Atmos. Sci.*, *29*, 959–970, 1972.

Reed, R. K., On estimating insolation over the ocean, *J. Phys. Oceanogr.*, *7*, 482–485, 1977.

Reed, R. K., and D. Halpern, Insolation and net long-wave radiation off the Oregon coast, *J. Geophys. Res.*, *80*(6), 839–844, 1975.

Ryznar, E., and M. R. Weber, Comments on "On the performance of pyranometers with silicon domes," *J. Appl. Meteorol.*, *21*, 1208–1210, 1982.

Seckel, G. R., and F. H. Beaudry, The radiation from sun and sky over the North Pacific Ocean (abstract), *Eos Trans. AGU*, *54*, 1114, 1973.

Simpson, J. J., and C. A. Paulson, Mid-ocean observations of atmospheric radiation, *Q. J. R. Meteorol. Soc.*, *105*, 487–502, 1979.

Tabata, S., Insolation in relation to cloud amount and sun's altitude, in *Studies on Oceanography*, edited by K. Yoshida, pp. 202–210, University of Tokyo Press, Tokyo, 1964.

TEMPO Group, Tyrrhenian Eddy Multi-Platform Observations 1989 experiment: Inventory of the measurements and preliminary results, *Tech. Rep. 1*, contract 0041-C, Ist. Fis. Atmos., Cons. Naz. Ric., Rome, 1991.

Weiss, A., On the performance of pyrgeometers with silicon domes, *J. Appl. Meteorol.*, *20*, 962–965, 1981.

F. Bignami, R. M. Leonardi, R. Santoleri, and M. E. Schiano, Istituto di Fisica dell'Atmosfera, CNR, P. Le Luigi Sturzo, 31, 00144 Rome, Italy.

E. Böhm, Earth Observation Division, Telespazio, Rome, Italy.

S. Marullo, ENEA, Centro Ricerche Ambiente Marino, via Anguillarese km 1.3, 00060 Santa Maria di Galeria (Rome), Italy.